NEOPLASIA
www.neoplasia.com

Volume 16 Number 5 May 2014 pp. 432–440 432

PARPi-FL - a Fluorescent PARP1 Inhibitor for Glioblastoma Imaging

Christopher P. Irwin*, Yasiri Portorreal*, Christian Brand*, Yachao Zhang*, Pooja Desai*, Beatriz Salinas*, Wolfgang A. Weber†,‡ and Thomas Reiner*,§

*Radiochemistry and Imaging Sciences Service, Department of Radiology, Memorial Sloan Kettering Cancer Center, New York, NY, 10065, USA; †Molecular Imaging and Therapy Service, Department of Radiology, Memorial Sloan Kettering Cancer Center, New York, NY, 10065, USA; ‡Molecular Pharmacology and Chemistry Program, Memorial Sloan Kettering Cancer Center, New York, NY, 10065, USA; §Center for Molecular Imaging and Nanotechnology, Memorial Sloan Kettering Cancer Center, New York, NY, 10065, USA

Abstract

New intravital optical imaging technologies have revolutionized our understanding of mammalian biology and continue to evolve rapidly. However, there are only a limited number of imaging probes available to date. In this study, we investigated in mouse models of glioblastoma whether a fluorescent small molecule inhibitor of the DNA repair enzyme PARP1, PARPi-FL, can be used as an imaging agent to detect glioblastomas *in vivo*. We demonstrated that PARPi-FL has appropriate biophysical properties, low toxicity at concentrations used for imaging, high stability *in vivo*, and accumulates selectively in glioblastomas due to high PARP1 expression. Importantly, subcutaneous and orthotopic glioblastoma xenografts were imaged with high contrast clearly defining tumor tissue from normal surrounding tissue. This research represents a step toward exploring and developing PARPi-FL as an optical intraoperative imaging agent for PARP1 in the clinic.

Neoplasia (2014) 16, 432–440

Introduction

Over the last decade, the DNA repair protein PARP1 has become a focal point of biomedical research [1–3]. The interest stems from the observation that human tumors deficient in the DNA repair enzymes BRCA1 or BRCA2 are often dependent on PARP1 DNA repair pathways. This makes the tumor cells susceptible to PARP1 inhibitors, a concept known as synthetic lethality. PARP1's value as a target for pharmaceutical intervention is reflected in the recent development of a variety of small molecule PARP1 inhibitors (e.g. ABT-888, Abbott; AG014699, Pfizer; AZD2281, Astra-Zeneca; BSI-201, Sanofi-Aventis; MK-4827, Merck).

Originating from the small molecule therapeutic AZD2281 (Olaparib), we synthesized PARPi-FL, a fluorescent small molecule inhibitor of PARP1 [4,5]. Specifically, the cyclopropane group of Olaparib was replaced by the green fluorescent BODIPY-FL to create the PARP1 imaging agent. Binding assays showed that the affinity of PARPi-FL (12.2 nM) [5] is very close to that of Olaparib (5 nM) [6], indicating that the addition of the BODIPY fluorophore does not result in an appreciable reduction in binding. This binding was shown to be rapid and selective to PARP1, similar to the parent compound Olaparib [4,5]. Additionally, it was shown on a cellular level that the imaging agent distributes quickly within tumor tissue and efficiently clears from the regions of low PARP1 expression within minutes [4].

High specific tumor uptake of PARPi-FL in window-chamber models of human cancer using confocal microscopy [4,7] suggested

Address all correspondence to: T. Reiner, PhD, Department of Radiology, Memorial Sloan Kettering Cancer Center, 1275 York Avenue, New York, NY 10065. E-mail: reinert@mskcc.org
Received 9 May 2014; Accepted 13 May 2014

1476-5586/14
http://dx.doi.org/10.1016/j.neo.2014.05.005

that optical imaging with PARPi-FL may also be promising for intraoperative detection of cancer in patients. PARPi-FL imaging could exploit the overexpression of PARP1 in various forms of cancer, including breast cancer [8–10], melanoma [11], and brain malignancies [12,13]. The overexpression of PARP1 is particularly apparent in brain malignancies because of the extremely sparse PARP1 expression in healthy brain. The high tumor expression and low healthy tissue expression of PARP1 suggest that it represents a valuable target for detection and staging of cancer, especially glioblastoma.

The detection and understanding of the genetic and molecular basis of glioblastoma by non-invasive imaging has advanced significantly over the last several decades, however progress in treatment options and survival for glioblastoma patients have been more limited [14]. While surgery combined with external beam radiotherapy is initially effective, almost all patients develop recurrent tumors within a few months. This is in part due to the diffuse, infiltrative growth of brain tumors, which makes it difficult to achieve microscopically complete resections. Nevertheless, several studies have shown that more complete resections prolong survival [15–17]. Therefore, with the advent of modern intravital imaging protocols [18], delineation of tumor tissue with a fluorescent probe *in vivo* in real time could represent a valuable tool for operating physicians, allowing more complete removal of tumor tissue.

In the current study, we hypothesized that PARPi-FL could ultimately represent a clinically useful intraoperative imaging agent for glioblastoma. To evaluate PARPi-FL for this use, we designed a series of experiments to address the following questions: 1) Does PARPi-FL show toxicity which would prevent its use as an imaging agent in the clinic? 2) Does PARPi-FL provide sufficient contrast for *in vivo* imaging? 3) Is uptake of PARPi-FL in cancer models correlated to PARP1 expression? 4) Are the kinetics of tumor uptake and clearance from normal brain compatible with clinical intraoperative imaging? We not only show that PARPi-FL is a highly selective probe, but that targeting of PARP1 can be used to identify glioblastomas. We envision that this imaging agent will ultimately be beneficial in the clinic by aiding the visualization of glioblastomas during surgery, helping to achieve more complete tumor resection.

Materials and Methods

Unless otherwise noted, all solvents and reagents were obtained from Sigma-Aldrich (St. Louis, MO) and did not undergo further purification. BODIPY-FL succinimidyl ester was purchased from Life Technologies (Carlsbad, CA). Olaparib (AZD2281) was purchased from LC Laboratories (Woburn, MA). PARPi-FL was synthesized as described earlier [5]. All high performance liquid chromatography (HPLC) purifications were performed on a Shimadzu UFLC HPLC system equipped with a DGU-20A degasser, a SPD-M20A UV detector, a LC-20AB pump system, a CBM-20A communication BUS module, a FRC-10A fraction collector, and a RF-20A xs fluorescence detector (excitation: 503 nm, emission: 515 nm) using reversed phase columns. A Phenomenex Jupiter column (5 μm C18, 300 Å, 250 × 10 mm) was used for semi-preparative purifications (3.5 mL/min, Buffer A: 0.1% trifluoroacetic acid (TFA) in water, Buffer B: 0.1% TFA in acetonitrile, 10 to 95% B in 18 min) and a Waters Atlantis T3 column (C18, 5 μm, 4.6 mm × 250 mm) was used for HPLC purifications (1.0 mL/min, Buffer A: 0.1% TFA in water, Buffer B: 0.1% TFA in acetonitrile, 5 to 95% B in 17 min).

Cell Culture

The human glioblastoma cell lines U87 MG and U251 MG were generously provided by the laboratory of Dr. Ronald Blasberg (MSKCC, New York, NY). Both cells lines were grown in Eagle's Minimal Essential Medium (MEM), 10% (vol/vol) heat inactivated fetal bovine serum, 100 IU penicillin, and 100 μg/mL streptomycin, purchased from the culture media preparation facility at Memorial Sloan Kettering Cancer Center (MSKCC New York, NY).

Mouse Models

Athymic nude NU/J mice from Jackson Laboratories (Bar Harbor, Maine) were used for imaging (n = 8) and pharmacokinetic studies (n = 48). Athymic nude CrTac:NCr-Foxn1^{nu} mice from Taconic Laboratories (Hudson, NY) were used to determine the stability of PARPi-FL (n = 18). They were further used for orthotopic mouse models (n = 24). For *in vivo* toxicology, B6D2F1 mice from Jackson Laboratories (Bar Harbor, Maine) were used. For subcutaneous injections, mice were anesthetized with 2% isoflurane gas in 2 L/min medical air. For orthotopic injections, mice were anesthetized with a 150 mg/kg ketamine and 15 mg/kg xylazine cocktail (10 μL/g). For all intravenous injections, mice were gently warmed with a heat lamp, placed on a restrainer, tail sterilized with alcohol pads, and the injection was placed into a lateral tail vein. All animal experiments were done in accordance with protocols approved by the Institutional Animal Care and Use Committee of MSKCC and followed National Institutes of Health guidelines for animal welfare.

Blood Half-life

The blood half-life of PARPi-FL was calculated by measuring the ear blood vessel fluorescence. Specifically, the mouse was anesthetized and placed on a heated stage of a Zeiss Lumar fluorescence dissection microscope. The ear was secured with tape and a catheter was inserted into the lateral tail vein. Once set up, time-lapse fluorescence imaging was performed from pre-injection through 120 minutes post intravenous injection of PARPi-FL (2.5 mg/kg in 200 μL of 19.5% 1:1 dimethylacetamide (DMAC):Kolliphor, 3.5% DMSO, 77% PBS). Rate capture for time-lapse imaging was 1 image/s until 5 minutes post injection and 12 images/hour for the remaining 115 minutes. Fluorescence intensity of the blood vessel in each image was quantified using ImageJ 1.47u image processing software. The blood half-life was calculated using Prism 6.0c (GraphPad Software, La Jolla, CA).

Hydrophobicity Index Determination

Chemical Hydrophobicity Index (CHI) was determined according to the procedures reported earlier [19]. Briefly, a series of standards with known CHIs were analyzed with reverse phase HPLC. Retention times of the standards along with their known CHIs were plotted with Prism 6.0c software. A line was fit to the data to create a calibration curve, which was then used to calculate the CHI of PARPi-FL based on the HPLC retention time.

In Vitro Toxicity

For MTT-based toxicology, a commercial MTT assay (Sigma Aldrich, St. Louis, MO) was performed according the manufacturer's instructions to measure the amount of living cells through quantification of the metabolic activity. Specifically, 2.5×10^3 U87 or 5×10^3 U251 glioblastoma cells were seeded per well in 96-well plates. Plates were incubated at 37 °C, and 24 hours later the media was aspirated and replaced with varying concentrations of PARPi-FL

A

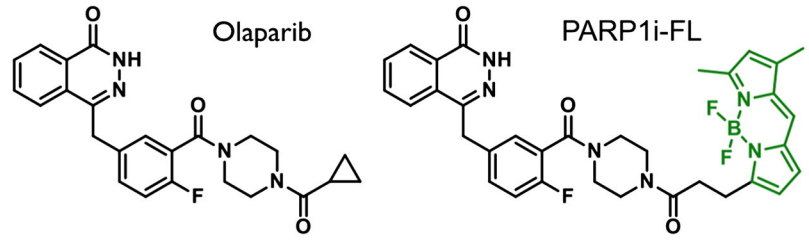

B

Biophysical Properties	Olaparib	PARPi-FL
EC_{50}	5 nM[a]	12.2 nM[b]
Abs_{max}/Em_{max}	N/A	507nm/525nm[c]
CHI	34.1	72.21
$logP_{CHI}$	0.8	2.9
protein binding	64.6% (+/- 5.0%)	99.2% (+/- 0.1%)[c]

Figure 1. Structure of Olaparib precursor and PARPi-FL biophysical properties. (A) Molecular structures of Olaparib and PARPi-FL. Green: fluorescent BODIPY-FL component of PARPi-FL; (B) Key pharmacokinetic parameters of PARPi-FL and Olaparib in mice; [a]Menear et al. 2008 [6], [b]Reiner et al. 2012 [5]; [c]Thurber et al. 2013 [4].

or Olaparib (100 μM, 33 μM, 10 μM, 3.3 μM, 1 μM, 0.3 μM, 0.1 μM, and 0.03 μM), each in triplicate. The plates were incubated for 7 days at 37 °C, after which the media was aspirated and replaced with 10% MTT solution in media. After incubation for 4 hours at 37 °C, an equal amount of MTT solubility solution was added. The absorbance levels were measured with SpectraMax M5 spectrophotometer with SoftMax Pro software, with absorbance at 570 nm and the background absorbance at 690 nm. Percent survival for U87 and U251 cells receiving different doses of PARPi-FL or Olaparib were determined by calculating the percent absorbance readings of their respective control wells.

Clonogenic proliferation assays were performed as reported earlier [20]. Briefly, U87 and U251 cells were separately seeded in 6-well plates (5×10^2 and 1×10^3 cells/well respectively) in 2 mL of complete media in 6 replicates and allowed to incubate at 37 °C. After 24 hours the media was replaced with complete media containing 10 μM PARPi-FL, 10 μM Olaparib, or with drug-free complete media. Cells were allowed to incubate for 24 hours at 37 °C, after which cells were washed with phosphate-buffered saline (PBS), and then incubated in drug-free complete media for 14 days. After incubation, the cells were stained with 0.5% crystal violet stain for 30 minutes then washed with water. The plates were air dried overnight and colony numbers were counted.

In Vitro and In Vivo Stability

The *in vitro* stability was assessed by incubating 10 μM PARPi-FL in human serum (Sigma-Aldrich, St. Louis, MO) for 0 to 24 hours at 37 °C. At 0 h, 0.25 h, 1 h, 2 h, 4 h, 8 h, 16 h and 24 h the sample was immediately placed on ice and mixed 1:1 with a solution of acetonitrile/DMSO (250 μL) and then vigorously vortexed for 30 seconds to precipitate out serum protein. The sample was centrifuged at 3000 RCF for 3 minutes at 4°C, and the supernatant collected. This procedure was repeated three times, and the combined supernatants analyzed by HPLC equipped with fluorescence detector (Shimadzu RF-20A xs). Concentrations of PARPi-FL in the samples were quantified by integrating the PARPi-FL peak using Prism 6.0c software. *In vivo* stability was assessed by collecting blood from nude mice sacrificed at 5 min, 15 min, 30 min, 45 min, and 90 min post intravenous injection of 2.5 mg/kg PARPi-FL in vehicle solution stated above. Plasma isolation, analysis, and quantification were done identically to *in vitro* serum stability analysis. Additionally, the fluorescent impurities of the samples were quantified by integrating the non-PARPi-FL fluorescent peaks.

In Vivo Toxicology

Toxicity was assessed by evaluating mortality, morbidity, clinical observations, weight, as well as hematological and clinical chemistry parameters in mice with the help of the Antitumor Assessment core facility at MSKCC. Four mice were injected intravenously with 2.5 mg/kg of PARPi-FL (in 200 μL of 19.5% 1:1 dimethylacetamide (DMAC):Kolliphor, 3.5% DMSO, 77% PBS) and 4 mice were injected with vehicle only. Two days after injection, the mice were sacrificed. At the time of sacrifice, blood samples were obtained and hematology analysis was performed with a Hemavet 950FS analyzer with the following parameters: white blood cell count (WBC), red blood cell count (RBC), hemoglobin concentration (HB), hematocrit (HCT), platelet count (PLT). Also at the time of sacrifice, blood samples were obtained for clinical chemistry analysis performed on a Beckman Coulter AU680 analyzer with the following parameters: alkaline phosphatase (ALP), alanine aminotransferase (ALT), aspartate aminotransferase (AST), gamma-glutamyl transpeptidase (GGT), albumin (ALB) and total bilirubin (TBIL).

Surface Fluorescence Imaging

While the cellular pharmacokinetics of PARPi-FL have been reported in the past [4,7], the macroscopic and organ-specific distribution has not been investigated so far. In order to determine the tissue distribution and systemic pharmacokinetics of PARPi-FL, mice were injected intravenously with the imaging agent, sacrificed at various time points, and the *ex vivo* organ epifluorescence was

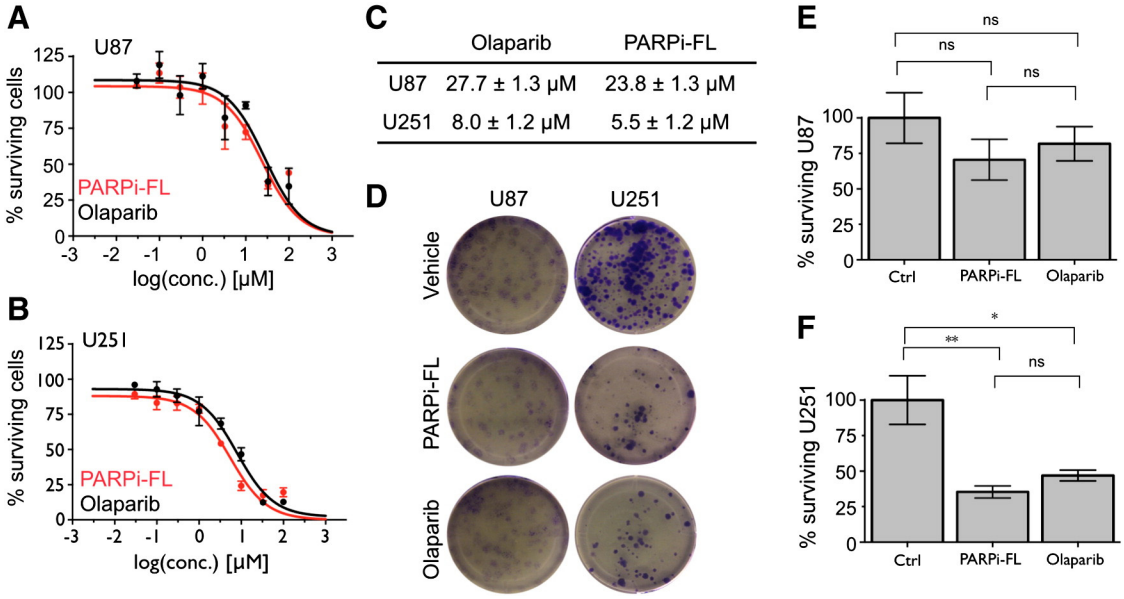

Figure 2. In vitro toxicity of PARPi-FL and Olaparib. (A,B) Percent of surviving U87 and U251 cells incubated with varying amounts of PARPi-FL or the parent drug Olaparib for 7 days based on MTT assays; (C) IC_{50} values obtained from MTT assays for U87 and U251, treated with PARPi-FL or Olaparib; (D) Representative images of clonogenic assay; (E) Percent surviving U87 cells or (F) U251 cells after incubation in 10 μM PARPi-FL or 10 μM Olaparib for 24 h based on clonogenic assays.

quantified at different time points. U87 or U251 cells were implanted subcutaneously (5×10^6 cells in 200 μL 1:1 PBS/Matrigel (BD Biosciences, San Jose, CA)) in the shoulders of 4 mice per time point and allowed to grow for approximately two weeks until the tumors reached 5–10 mm in size. Thereafter, for each time point 2.5 mg/kg PARPi-FL (in 200 μL 19.5% DMAC: kolliphor, 3.5% DMSO, 77% PBS) was injected intravenously via lateral tail vein in 3 mice and vehicle (200 μL of 19.5% DMAC: kolliphor, 3.5% DMSO, 77% PBS) into one mouse. The cohorts of mice were then sacrificed at select time points from 5 to 720 minutes post injection. Tumor, brain, and muscle tissues were harvested post mortem, placed on a petri dish and fluorescence imaged with a Maestro imaging system. The PARPi-FL emission spectrum was used to separate out the PARPi-FL signal from background fluorescence. Regions of interest were drawn around each organ to calculate the average fluorescence intensity. From this data, the increase in fluorescence (difference between vehicle injected mouse organs and PARPi-FL injected organs) was calculated and plotted with GraphPad Prism 6.0c. For subcutaneous blocking studies, U87 cells were implanted and grown in mice as stated above. The mice were injected with PARPi-FL as stated above, with the exception that 4 mice were injected with 125 mg/kg olaparib (in 100 μL of 7.5% DMSO, 12.5% Cremophor, 80% PBS) prior to injection of PARPi-FL, 4 mice were injected with vehicle (100 μL of 7.5% DMSO, 12.5% Cremophor, 80% PBS) prior to injection of PARPi-FL, and 2 mice were injected with vehicle only. All injections were 30 min prior to the injection of the imaging agent. Imaging and analysis for the blocking study was performed with the IVIS spectrum fluorescence imaging system (PerkinElmer) and Living Image 4.4 software.

Western Blots

For Western blots, tumors, muscle and brain were homogenized in 400 μL of 1x radioimmunoprecipitation assay buffer and 2x Mini Complete Protease Inhibitor Cocktail tablet (Roche, Indianapolis, IN). The samples were spun at 4 °C at 10,000 rpm for 10 minutes, and the supernatant was collected. Protein concentration was measured using a bicinchoninic acid protein assay according to the manufacturer's instructions (Thermo Scientific, Waltham, MA). Tumor lysate (30 μg) was loaded onto NuPAGE Novex 4% to 12% Bis-Tris 1.0-mm gels, and electrophoresis was performed with the XCell SureLock Mini-Electrophoresis system (both Invitrogen). Protein was transferred using the iBlot Dry Blotting System to a nitrocellulose membrane (Invitrogen). The blot was then blocked in 5% nonfat milk for 1 hour, washed with 1 × TBS-Tween 20 (Boston BioProducts, Ashland, MA), and incubated overnight at 4 °C with 1:1000 anti-PARP-1/2 in 5% nonfat milk (Santa Cruz Biotechnology). After three 10 minute washes with 1 × TBS-Tween 20, blots were incubated with 1:10,000 goat-anti-rabbit horseradish peroxidase-conjugated secondary antibody (Jackson ImmunoResearch, West Grove, PA) at room temperature for 1 hour. After three 10 minute washes with 1 × TBS-Tween 20, blots were incubated with SuperSignal West Pico Chemiluminescent Substrate (Thermo Scientific), exposed for 3 minutes, and then processed with the Kodak (Rochester, NY) X-OMAT 2000A processor. For β-Actin, the same blot was stripped with restore WB stripping buffer (Thermo scientific). After three 5 min washes with TBS-Tween20 the blot was blocked with 5% nonfat milk in TBS-Tween20 for an hour at room temperature. After blocking, the blots were incubated for 1 hour at room temperature with 1:5000 anti-β-Actin (Sigma-Adrich, St Louis, MO) in 5% nonfat milk (R&D Systems, Minneapolis, MN). After three 10 min washes with 1 × TBS-Tween 20, blots were incubated with 1:10,000 rabbit-anti-mouse horseradish peroxidase-conjugated secondary antibody at room temperature for 1 hour. After three 10 min washes with 1 × TBS-Tween 20, blots were incubated with SuperSignal West Pico Chemiluminescent Substrate (Thermo Scientific), exposed for 10 seconds, and then processed with the Kodak X-OMAT 2000A processor.

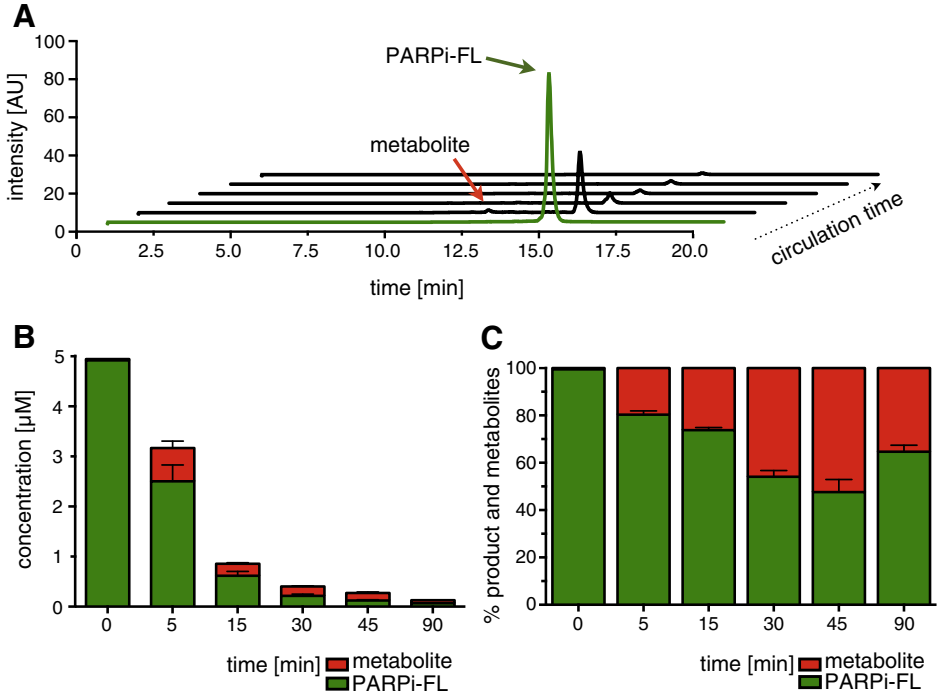

Figure 3. Metabolic stability of PARPi-FL. (A) Fluorescence-HPLC trace of PARPi-FL (green) and metabolites (red) in mouse blood at different time points post injection of PARPi-FL (200 μL of 19.5% 1:1 dimethylacetamide (DMAC):Kolliphor, 3.5% DMSO, 77% PBS); (B) Concentration of PARPi-FL and metabolites at different time points post injection; (C) Percent intact PARPi-FL in mouse blood at different time points after injection.

Orthotopic Brain Tumors

U87 cells (5×10^4 in 20 µL PBS) were implanted into the brains of mice and allowed to grow for approximately 3 weeks. Tumor-bearing mice and healthy control mice were injected intravenously with 2.5 mg/kg of PARPi-FL (in 200 µL 19.5% DMAC:kolliphor, 3.5% DMSO, 77% PBS) and sacrificed 1 hour later. The brains of the mice were harvested, then imaged and analyzed with IVIS spectrum fluorescence imaging system (PerkinElmer) and Living Image 4.4 software. Histology was performed by freezing the brains in O.C.T. compound (Sakura Finetek USA, Inc., Torrance, CA) on dry ice. Tissue sections where created by slicing serial 6 µm sections of the frozen brains. Staining with hematoxylin and eosin (H&E) and imaging were done with the assistance of the Molecular Cytology Core Facilities at MSKCC. The size and location of each orthotopic tumor was documented for each tumor-bearing brain with the assistance of the Pathology Core Facilities at MSKCC. This protocol was repeated for orthotopic blocking studies, with the exception that mice received a dose of either 125 mg/kg olaparib (in 100 µL of 7.5% DMSO, 12.5% Cremophor, 80% PBS) or vehicle (100 µL of 7.5% DMSO, 12.5% Cremophor, 80% PBS) 30 min prior to injection of PARPi-FL.

Statistical Analysis

Unpaired t-tests were done to determine statistical difference. $P < 0.05$ was considered statistically significant. Data is presented as mean ± SEM or mean ± SD.

Results

The molecular structure of PARPi-FL is based on Olaparib (Figure 1*B*, [5,6]). The small molecule fluorescent imaging agent is cleared rapidly from the blood in mice with an alpha half-life of 1.2 min and a beta half-life of 88.2 min, resulting in a weighted blood half-life $t_{1/2}$ of 24.5 min. The chemical hydrophobicity index (CHI) is 72.21, which corresponds to a $\log P_{CHI}$ of 2.9, a value that is higher than the CHI of its parent compound Olaparib (CHI = 34.1, $\log P_{CHI}$ = 0.8). And although the hydrophobicity of PARPi-FL results in a higher plasma protein binding (64.6 ± 5.0 and 99.2 ± 0.1 for olaparib and PARPi-FL, respectively), we were able to show in the past that PARPi-FL selectively targets PARP1, similar to its parent compound, both *in vitro* as well as *in vivo* [4,5]. The $\log P_{CHI}$ of PARPi-FL compares well with other small molecule drugs, including drugs that are available in the central nervous system [21].

We investigated the toxicity profile of PARPi-FL in glioblastoma cell lines using MTT as well as clonogenic assays. For the MTT assays we incubated cells with either PARPi-FL or Olaparib at concentrations between 30 nM and 0.1 mM for 7 days. In the glioblastoma cell lines U87 and U251, PARPi-FL has similar toxicity to Olaparib (Figure 2, *A* and *C*). The IC_{50} of PARPi-FL was calculated to be slightly lower than Olaparib (27.7 ± 1.3 µM and 23.8 ± 1.3 µM, respectively, for U87; 8.0 ± 1.2 µM and 5.5 ± 1.2 µM, respectively, for U251). MTT-based assays indicate that both PARPi-FL and Olaparib are more toxic to U251 cells than U87 cells (Figure 2, *B* and *C*). The obtained IC_{50} values of Olaparib are within the range of those obtained previously for different cell lines (IC_{50} = 1.0 µM – 33.8 µM [22]), supporting the validity of the results seen here. In order to further analyze the *in vitro* toxicity of PARPi-FL, clonogenic assays were also performed. PARPi-FL and Olaparib demonstrated a similar reduction in the number of surviving colonies for both U87 and U251 cells (Figure 2, *E* and *F*). When tested on U87 cells, both PARPi-FL and Olaparib decreased the number of surviving colonies by 20-30%. (P = 0.23, and P = 0.42 compared with vehicle, respectively, Figure 2*E*). When tested on U251 cells, both PARPi-FL

and Olaparib caused a significant reduction in the number of surviving cells (Figure 2*F*). Normalized to control, the cell survival rate in PARPi-FL was 35.3% ($P < .001$) and Olaparib was 46.9% ($P = .013$). Given that the results from the *in vitro* toxicity assessment indicated similar toxicity levels in PARPi-FL and Olaparib, we next sought to evaluate the toxicity of PARPi-FL *in vivo*. Following injection of 2.5 mg/kg PARPi-FL or vehicle, none of the mice showed signs of sickness or distress from PARPi-FL based on clinical observations of behavioral and physical indicators, and all mice survived until their endpoints (48 h). At the end point of the study, no hematological or clinical chemistry measurements indicated that PARPi-FL had immediate adverse effects to the health of the mice (Supplementary Table S1).

Similar to radioactive tracers, the stability of an imaging agent *in vivo* is essential for its use. Therefore, we aimed to determine if there were any major fluorescent degradation products that could be observed during imaging. In human serum (37 °C), the drug showed no degradation over the course of 24 hours (Supplementary Figure S1). After injection in mice (2.5 mg/kg in 200 µL of 19.5% 1:1 dimethylacetamide (DMAC):Kolliphor, 3.5% DMSO, 77% PBS), blood samples were obtained between 5 and 90 minutes post injection and the compound and impurities were quantified using an HPLC equipped with a fluorescence detector. Throughout the series, impurity peaks were seen between 8.0 and 14.0 minutes of retention time, whereas the pure compound peak was detected at 14.3 minutes (Figure 3*A*). The concentration of product and impurities at each time point were calculated by integrating the product or impurities peaks in their respective time frames, then converting to concentration by using a calibration curve (Figure 3*B*). Even after 30 min of circulation, more than 54.1 ± 5.9 % of the compound is intact (Figure 3*C*). More significantly, during the initial uptake phase of PARPi-FL into tissue (0 min – 5 min), the vast majority of the compound is intact (80.3%, SEM = 1.6%). Notably, there are more than 10 metabolite peaks, each of them making up only a small fraction of the total fluorescent signal. The large number of metabolites makes the identification of individual small peaks difficult, particularly at later time points. This indicates that the cellular uptake and fluorescent signal produced by PARPi-FL and observed in earlier imaging studies [4,7] likely originates from the original PARP1 inhibitor, indicating the compound to have a suitable stability for further investigation.

Ex vivo epifluorescence imaging of PARPi-FL measured by *ex vivo* showed that after an initial clearing phase (0 min – 30 min, Figure 4), PARPi-FL is retained in U87 tumors (Figure 4*A*) at much higher levels and longer than healthy brain (Figure 4*B*) or muscle (Figure 4*C*) post intravenous injection. Specifically, at 90 minutes post intravenous injection, the concentration of PARPi-FL in tumor (mean AU/px = 20.49, SEM = 3.68) was markedly higher than muscle (mean AU/px = 3.45, SEM = 0.45) or brain (mean AU/px = 0.13, SEM = 0.10), indicating that PARPi-FL is capable of generating high contrast images of tumor tissue in the brain. For optical imaging, a window between 60 minutes and 180 minutes post injection is ideal. We have shown in earlier works [4,5] that this provides a long enough time for the imaging agent to accumulate in the nucleus as well as to clear from the vasculature, extracellular and perinuclear space, allowing PARP1-specific optical imaging.

Uptake of PARPi-FL by U251 tumors was lower than in U87 tumors, but also markedly higher than of normal brain and muscle (Figure 5). Western blot analyses (Figure 5*C*) showed greater

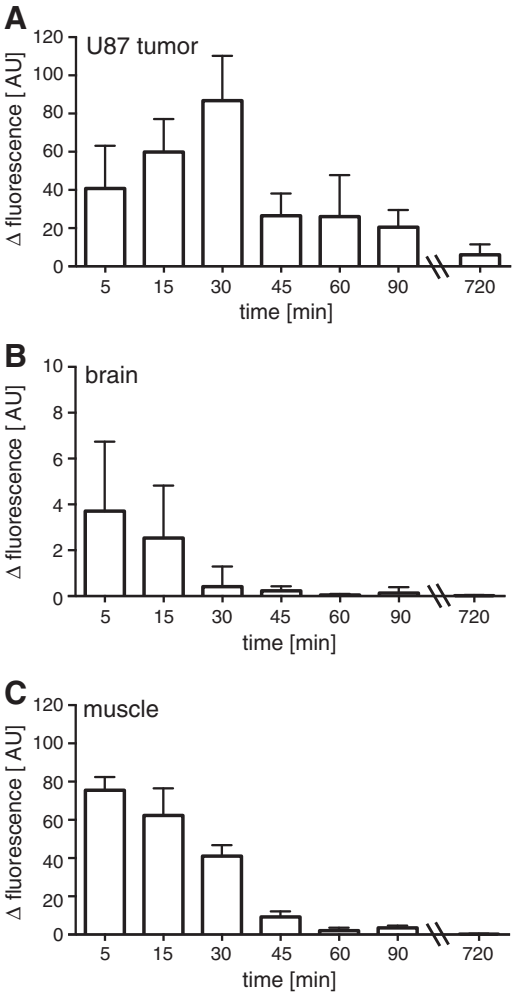

Figure 4. Pharmacokinetics of PARPi-FL in mice. (A) U87 tumor, (B) brain and (C) muscle fluorescence intensities above baseline measured from 5 to 720 minutes after injection of PARPi-FL (200 µL of 19.5% 1:1 DMAC:Kolliphor, 3.5% DMSO, 77% PBS). Baseline fluorescence was determined by imaging nude mice injected with vehicle only.

expression of PARP1 in tumor tissue compared to normal muscle or brain tissues, correlating to the PARPi-FL signal. The differences in PARPi-FL uptake between U87 and U251 xenografts could be influenced by variabilities in vascular permeability, tissue perfusion or other factors influenced by the tumor microenvironment. In order to probe the specificity of PARPi-FL uptake in xenografts, we intravenously injected a 50-fold excess of olaparib into U87 xenograft-bearing mice 30 minutes prior to the injection of PARPi-FL. This reduced the uptake of the fluorescent imaging agent by 79% ($P = 0.002$), confirming that PARPi-FL is targeting PARP1 (Figure 6, *A-B*). High resolution fluorescence imaging showed that PARPi-FL indeed accumulates in cell nuclei, resulting in staining patterns similar to those observed before (Supplementary Figure 6*C*, [4,5]).

In addition to subcutaneous xenografts, we used orthotopic mouse models for PARPi-FL imaging. PARPi-FL was injected into groups of orthotopic tumor-bearing and healthy mice, which were sacrificed 1 hour post injection for *ex vivo* imaging of the brains (Figure 7). Mice bearing orthotopic tumors showed significantly higher uptake of PARPi-FL than healthy mice injected with the imaging agent

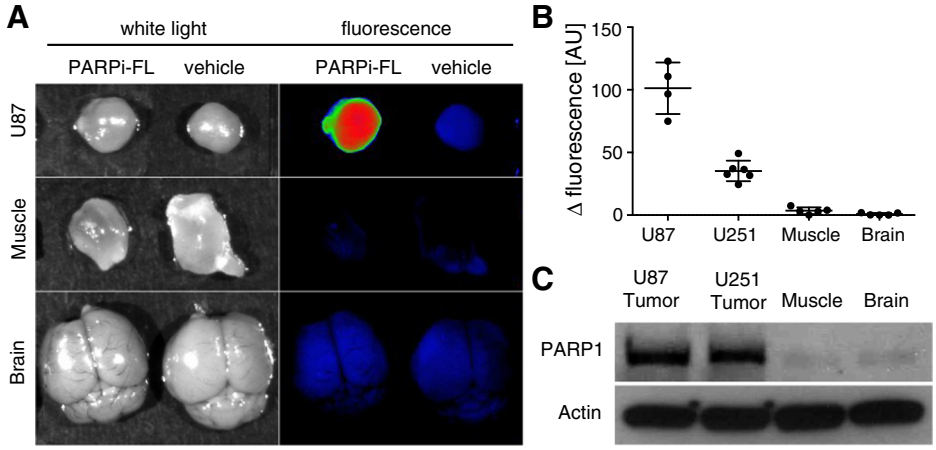

Figure 5. PARPi-FL tumor accumulation and PARP1 expression. (A) Representative images of tumor, muscle and brain tissue 2 h after injection of PARPi-FL (200 μL of 19.5% 1:1 DMAC:Kolliphor, 3.5% DMSO, 77% PBS) or vehicle only imaged *ex vivo*; (B) Fluorescence quantification of U87 xenograft, U251 xenograft, muscle and brain tissue; (C) PARP1 Western Blot of imaged organs.

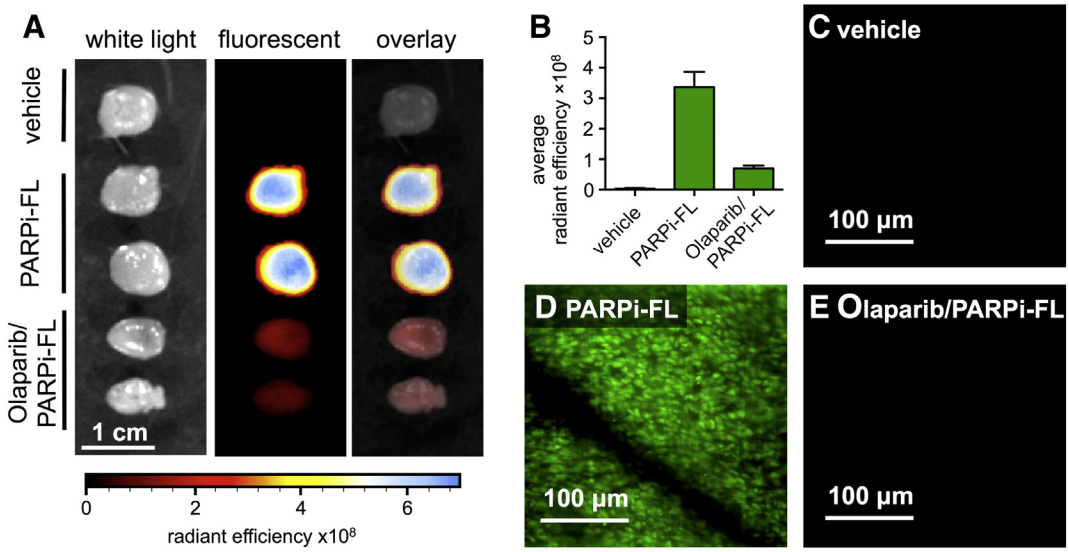

Figure 6. PARPi-FL imaging of U87 tumors with and without prior injection of olaparib. (A) Representative white light, fluorescence, and overlay images of U87 tumor tissues which were injected with either vehicle alone, PARPi-FL (2.5 mg/kg, 200 μL of 19.5% 1:1 DMAC: Kolliphor, 3.5% DMSO, 77% PBS) or olaparib/PARPi-FL (125 mg/kg olaparib in 100 μL of 7.5% DMSO, 12.5% Cremophor, 80% PBS, followed 30 minutes later by 2.5 mg/kg PARPi-FL in 200 μL of 19.5% 1:1 DMAC:Kolliphor, 3.5% DMSO, 77% PBS); (B) Fluorescence quantification of U87 xenografts from panel 6A; (C–E) Fluorescence microscope imaging of tumor tissues in panel 6A, confirming nuclear uptake of PARPi-FL in non-blocked tumor tissues, but not in the vehicle or Olaparib pre-treatment groups.

(Figure 7*A*). Similar to experiments with mice bearing xenograft tumors, we were able to suppress the uptake of PARPi-FL in mice which were injected with olaparib prior to PARPi-FL (Supplementary Figure S2*A*). High resolution imaging of a mouse brain bearing an orthotopic U87 glioblastoma furthermore showed that the uptake of PARPi-FL in the tumor is nuclear (Supplementary Figure S2), similar to the uptake patterns observed previously (Figure 6*C*). In healthy areas of a brain bearing an orthotopic U87 tumor, no nuclear staining of the cells was observable. In a two-dimensional non-background corrected fluorescence intensity profile, tumor-bearing brain tissue showed a large increase in fluorescence (maximum radiant efficiency = 5.0×10^8) in the area of tumor tissue, as opposed to non-tumor-bearing brain tissue which showed little fluorescence across the length of the brain (maximum radiant efficiency = 0.5×10^8) and was only slightly greater than that of background fluorescence (max radiant efficiency = 0.3×10^8, Figure 7*B*). Following imaging, the mouse brains were frozen and histological sections were prepared for H&E staining. The presence and location was then confirmed to correspond well with the areas of highest fluorescence intensity (Figure 7*C*).

Discussion

The National Cancer Institute estimates that 23,380 adults (12,820 men and 10,560 women) will be diagnosed with brain and other

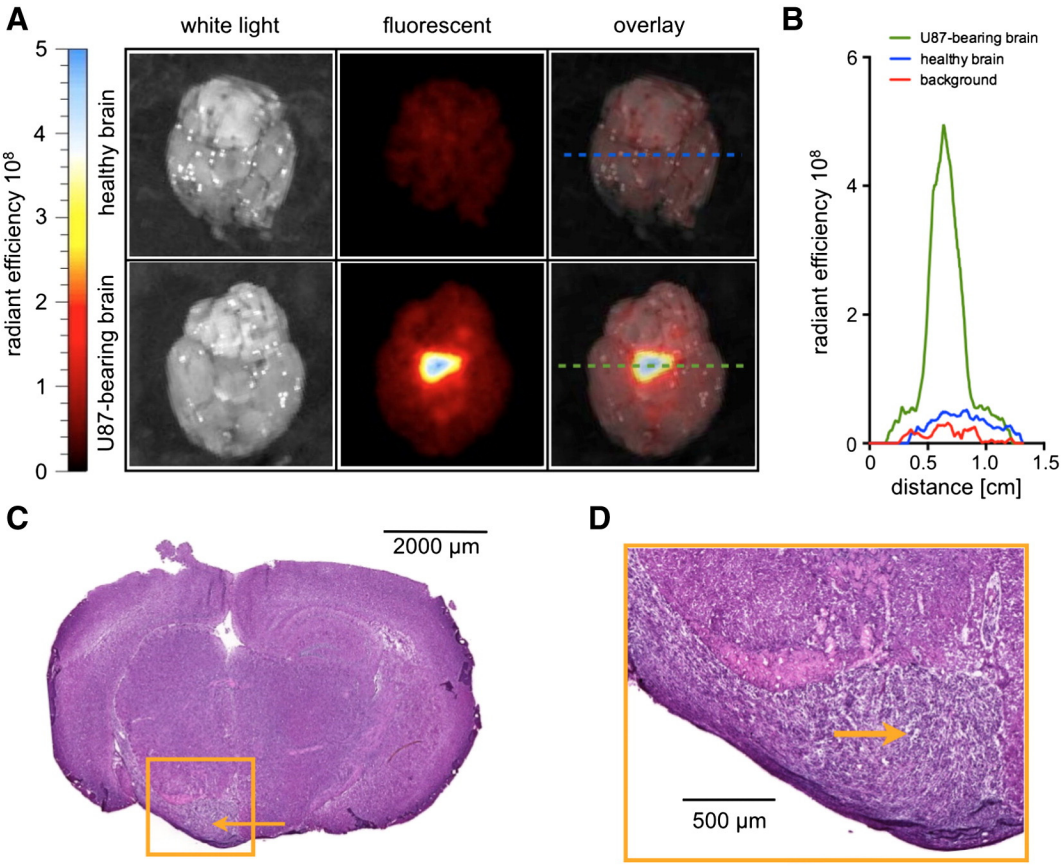

Figure 7. Orthotopic brain tumor imaging with PARPi-FL. (A) White light, fluorescence, and overlay images of healthy brain and orthotopic tumor-bearing brain imaged with an IVIS spectrum fluorescence imaging system 1 hour post intravenous injection (200 μL of 19.5% 1:1 DMAC:Kolliphor, 3.5% DMSO, 77% PBS); (B) Profile plot of fluorescence intensity across orthotopic tumor-bearing brain, healthy brain, and background; (C) H&E stained tumor-bearing brain section from A; (D) High resolution image of tumor shown in C; Radiant efficiency = (emission light (photons/sec/cm^2/str))/(excitation light (mW/cm^2)).

nervous system tumors in 2014 in the United States alone. Glioblastoma is a particularly aggressive and invasive form of brain cancer, and the median survival ranges from 31.9 months for patients 20–29 years of age to only 5.6 months in patients 80 years and older [23]. One method for improving median survival in glioblastoma patients is to increase the completeness of tumor tissue resected during surgery, while not increasing the amount of healthy brain tissue removed [17,24]. In clinical practice however, the distinction between malignant growth and healthy brain tissue can be difficult to make, and the resection of healthy brain increases the incidence of post-surgical morbidity. To aid surgeons in distinguishing malignant tissue from normal brain tissue, intraoperative MRI [25] as well as fluorescence-guided surgery with the use of 5-aminolevulinic acid [26] have been utilized with some success. Still, progression-free survival is only modestly improved with the use of these techniques [25,26]. There is thus a need for better tools for intraoperative imaging [27,28]. In order to expand the portfolio of potential clinically relevant intraoperative probes, we investigated the potential of PARPi-FL to act as an agent to macroscopically delineate between high PARP1 and low PARP1 expressing tissues. Our aim was to evaluate the biophysical properties, *in vitro* and *in vivo* toxicity, pharmacokinetics, as well as the potential of PARPi-FL as a glioblastoma imaging agent in mouse xenograft models.

The compound was found to have a toxicity profile comparable to that of Olaparib, which is currently being used in phase III clinical trials. The maximum tolerated dose of Olaparib in humans (400 mg, twice daily) [29] is likely much greater than the dose that would be required for imaging in human patients using PARPi-FL. In comparison, intraoperative imaging with indocyanine green requires one dose of only 500 µg/kg or 35 mg per patient [30]. Similar concentrations of PARPi-FL are unlikely to induce adverse events.

In vivo organ epifluorescence studies indicate that PARPi-FL accumulates in U87 subcutaneous xenografts in much higher concentrations than in muscle or brain tissue, generating signal/noise ratios in excess of 10/1. We therefore believe that the high PARPi-FL uptake in glioblastoma could be used to generate a clearly detectable signal in tumor tissue against normal brain.

In summary, the data presented in this study indicate that the fluorescent imaging agent PARPi-FL has significant potential for fluorescence-assisted intraoperative imaging of glioblastoma. Additionally, because PARP1 is also upregulated in several other malignancies, PARP1 imaging agents may be useful for the delineation of not only glioblastoma, but also other primary cancers [8–11]. We envision their use during intraoperative procedures, non-invasive tumor diagnostics during endoscopic procedures, and even analysis of biopsy samples.

Supplementary data to this article can be found online at http://dx.doi.org/10.1016/j.neo.2014.05.005.

Acknowledgements

The authors thank the Small Animal Imaging Core, in particular Valerie Longo and Dr. Pat Zanzonico, the Anti Tumor Assessment Core, in particular Dr. Christopher Scull and Dr. Elisa de Stanchina, and the Pathology Core for support, in particular Dr. Sabastien Monette (P30 CA008748). Additionally, we would like to thank the MSKCC Metastasis Research Center for a Shared Resources Grant that provided funding support for the purchase of the IVIS Spectrum, and additional support from the Radiochemistry and Molecular Imaging Probes Core at Memorial Sloan-Kettering Cancer Center (P30 CA008748). The authors would also like to thank Dr. Jason S. Lewis, Dr. Sean Carlin, Dr. NagaVaraKishore Pillarsetty and Dr. Ronald G. Blasberg for helpful discussions. Finally, the authors thank the NIH (K25 EB016673 for T.R.), the Brain Tumor Center of Memorial Sloan Kettering Cancer Center (for T.R.) and the Radiology Development Fund (for T.R.) for their generous funding.

References

[1] Rouleau M, Patel A, Hendzel MJ, Kaufmann SH, and Poirier GG (2010). PARP inhibition: PARP1 and beyond. *Nat Rev Cancer* **10**, 293–301.

[2] Gradwohl G, Menissier de Muricia J, Molinete M, Simonin F, Koken M, Hoeumakers J, and de Muricia G (1990). The second zinc-finger domain of poly (ADP-ribose) polymerase determines the specificity for single-stranded breaks in DNA. *Proc Natl Acad Sci U S A* **87**, 2990–2994.

[3] Hassa PO and Hottiger MO (2008). The diverse biological roles of mammalian PARPS, a small but powerful family of poly-ADP-ribose polymerases. *Front Biosci* **12**, 3046–3082.

[4] Thurber GM, Yang KS, Reiner T, Kohler RH, Sorger P, Mitchison T, and Weissleder R (2013). Single-cell and subcellular pharmacokinetic imaging allows insight into drug action in vivo. *Nat Commun* **4**, 1505–1513.

[5] Reiner T, Lacy J, Keliher EJ, Yang KS, Ullal A, Kohler RH, Vinegoni C, and Weissleder R (2012). Imaging Therapeutic PARP Inhibition In Vivo through Bioorthogonally Developed Companion Imaging Agents. *Neoplasia* **14**, 169–177.

[6] Menear KA, Adcock C, Boulter R, Cockcroft XL, Copsey L, Cranston A, Dillon KJ, Drzewiecki J, Garman S, and Gomez S, et al (2008). 4-[3-(4-cyclopropanecarbonylpiperazine-1-carbonyl)-4-fluorobenzyl]-2H-phthalazin- 1-one: a novel bioavailable inhibitor of poly(ADP-ribose) polymerase-1. *J Med Chem* **51**, 6581–6591.

[7] Thurber G, Reiner T, Yang K, Kohler R, and Weissleder R (2014). Effect of Small Molecule Modification on Single Cell Pharmacokinetics of PARP Inhibitors. *Mol Cancer Ther* **13**, 986–995.

[8] Ossovskaya V, Koo IC, Kaldjian EP, Alvares C, and Sherman BM (2010). Upregulation of Poly (ADP-Ribose) Polymerase-1 (PARP1) in Triple-Negative Breast Cancer and Other Primary Human Tumor Types. *Genes Cancer* **1**, 812–821.

[9] Bieche dM and Linderau R (1996). Poly(ADP-ribose) polymerase gene expression status and genomic instability in human breast cancer. *Clin Cancer Res* **2**, 1163–1167.

[10] Rojo F, Garcia-Parra J, Zazo S, Tusquets I, Ferrer-Lozano J, Menendez S, Eroles P, Chamizo C, Servitja S, and Ramirez-Merino N, et al (2012). Nuclear PARP-1 protein overexpression is associated with poor overall survival in early breast cancer. *Ann Oncol* **23**, 1156–1164.

[11] Staibano S, Pepe S, Lo Muzio L, Somma P, Mascolo M, Argenziano G, Scalvenzi M, Salvatore G, Fabbrocini G, and Molea G, et al (2005). Poly (adenosine diphosphate-ribose) polymerase 1 expression in malignant melanomas from photoexposed areas of the head and neck region. *Hum Pathol* **36**, 724–731.

[12] Galia A, Calogero AE, Condorelli R, Fraggetta F, La Corte A, Ridolfo F, Bosco P, Castiglione R, and Salemi M (2012). PARP-1 protein expression in glioblastoma multiforme. *Eur J Histochem* **56**, 45–48.

[13] Barton VN, Donson AM, Kleinschmidt-DeMasters BK, Gore L, Liu AK, and Foreman NK (2009). PARP1 expression in pediatric central nervous system tumors. *Pediatr Blood Cancer* **53**, 1227–1230.

[14] Wen YP, Kesari S, Chattopadhyay R, Naidu CV, and Izumi T (2008). Malignant Gliomas in Adults. *N Engl J Med* **359**, 492–507.

[15] Kreth FW, Thon N, Simon M, Westphal M, Schackert G, Nikkhah G, Hentschel B, Reifenberger G, Pietsch T, and Weller M, et al (2013). Gross total but not incomplete resection of glioblastoma prolongs survival in the era of radiochemotherapy. *Ann Oncol* **24**, 3117–3123.

[16] Felsberg J, Rapp M, Loeser S, Fimmers R, Stummer W, Goeppert M, Steiger HJ, Friedensdorf B, Reifenberger G, and Sabel MC (2009). Prognostic significance of molecular markers and extent of resection in primary glioblastoma patients. *Clin Cancer Res* **15**, 6683–6693.

[17] Stummer W, Reulen HJ, Meinel T, Pichlmeier U, Schumacher W, Tonn JC, Rohde V, Oppel F, Turowski B, and Woiciechowsky C, et al (2008). Extent of resection and survival in glioblastoma multiforme: identification of and adjustment for bias. *Neurosurgery* **62**, 564–576.

[18] Pittet MJ and Weissleder R (2011). Intravital imaging. *Cell* **147**, 983–991.

[19] Valko K, Bevan C, and Reynolds D (1997). Chromatographic Hydrophobicity Index by Fast-Gradient RP-HPLC: A High-Throughput Alternative to log P/log D. *Anal Chem* **69**, 2022–2029.

[20] Munshi AHM and Meyn RE (2005). Clonogenic cell survival assay. *Methods Mol Med* **110**, 21–28.

[21] Lenz HPaGR (2005). Medicinal Chemical Properties of Successful Central Nervous System Drugs. *NeuroRx* **2**, 541–553.

[22] Norris RE, Adamson PC, Nguyen VT, and Fox E (2014). Preclinical evaluation of the PARP inhibitor, olaparib, in combination with cytotoxic chemotherapy in pediatric solid tumors. *Pediatr Blood Cancer* **61**, 145–150.

[23] Johnson DR and O'Neill BP (2012). Glioblastoma survival in the United States before and during the temozolomide era. *J Neurooncol* **107**, 359–364.

[24] Chen B, Wang H, Ge P, Zhao J, Li W, Gu H, Wang G, Luo Y, and Chen D (2012). Gross total resection of glioma with the intraoperative fluorescence-guidance of fluorescein sodium. *Int J Med Sci* **9**, 708–714.

[25] Senft C, Bink A, Franz K, Vatter H, Gasser T, and Seifert V (2011). Intraoperative MRI guidance and extent of resection in glioma surgery: a randomised, controlled trial. *Lancet Oncol* **12**, 997–1003.

[26] Stummer W, Pichlmeier U, Meinel T, Wiestler OK, Zanella F, and Reulen HJ (2006). Fluorescence-guided surgery with 5-aminolevulinic acid for resection of malignant glioma: a randomised controlled multicentre phase III trial. *Lancet Oncol* **7**, 392–401.

[27] Jarzabek MA, Sweeney KJ, Evans RL, Jacobs AH, Stupp R, O'Brien D, Berger MS, Prehn JH, and Byrne AT (2013). Molecular imaging in the development of a novel treatment paradigm for glioblastoma (GBM): an integrated multidisciplinary commentary. *Drug Discov Today* **18**, 1052–1066.

[28] Benezra M, Penate-Medina O, Zanzonico PB, Schaer D, Ow H, Burns A, DeStanchina E, Longo V, Herz E, and Iyer S, et al (2011). Multimodal silica nanoparticles are effective cancer-targeted probes in a model of human melanoma. *J Clin Invest* **121**, 2768–2780.

[29] Yamamoto N, Nokihara H, Yamada Y, Goto Y, Tanioka M, Shibata T, Yamada K, Asahina H, Kawata T, and Shi X, et al (2012). A Phase I, dose-finding and pharmacokinetic study of olaparib (AZD2281) in Japanese patients with advanced solid tumors. *Cancer Sci* **103**, 504–509.

[30] Kokudo N and Ishizawa T (2012). Clinical Application of Fluorescence Imaging of Liver Cancer Using Indocyanine Green. *Liver Cancer* **1**(1), 15–21.